J Biomol NMR (2012) 54:401–413
DOI 10.1007/s10858-012-9684-8

ARTICLE

Characterization of the ground state dynamics of proteorhodopsin by NMR and optical spectroscopies

Jochen Stehle · Frank Scholz · Frank Löhr · Sina Reckel · Christian Roos · Michaela Blum · Markus Braun · Clemens Glaubitz · Volker Dötsch · Josef Wachtveitl · Harald Schwalbe

Received: 28 August 2012 / Accepted: 2 November 2012 / Published online: 17 November 2012

Abstract We characterized the dynamics of proteorhodopsin (PR), solubilized in diC7PC, a detergent micelle, by liquid-state NMR spectroscopy at T = 323 K. Insights into the dynamics of PR at different time scales could be obtained and dynamic hot spots could be identified at distinct, functionally relevant regions of the protein, including the BC loop, the EF loop, the N-terminal part of helix F and the C-terminal part of helix G. We further characterize the dependence of the photocycle on different detergents (n-Dodecyl β-D-maltoside DDM; 1,2-diheptanoyl-sn-glycero-3-phosphocholine diC7PC) by ultrafast time-resolved UV/VIS spectroscopy. While the photocycle intermediates of PR in diC7PC and DDM exhibit highly similar spectral characteristics, significant changes in the population of these intermediates are observed. In-situ NMR experiments have been applied to characterize structural changes during the photocycle. Light-induced chemical shift changes detected during the photocycle in diC7PC are very small, in line with the changes in the population of intermediates in the photocycle of proteorhodopsin in diC7PC, where the late O-intermediate populated in DDM is missing and the population is shifted towards an equilibrium of intermediates states (M, N, O) without accumulation of a single populated intermediate.

Keywords Proteorhodopsin · Photocycle · Membrane protein dynamics · NMR spectroscopy

Abbreviations

PR	Proteorhodopsin
BR	Bacteriorhodopsin
FT	Fourier transform
IR	Infrared
diC7PC	1,2-diheptanoyl-sn-glycero-3-phosphocholine
DDM	*n*-Dodecyl β-D-maltoside
NMR	Nuclear magnetic resonance
MES	2-(*N*-morpholino)ethanesulfonic acid
SRII	Sensory rhodopsin II
UV	Ultra violet

Introduction

Light is one of the most interesting environmental factors; it plays a prominent role in information and energy transfer in nature. It triggers numerous signaling cascades, provides energy directly or indirectly for basically all biological systems and plays a major role in sensing environmental changes and in perception. An amazing variety of systems has evolved that interact with light. One extraordinary example of such a system is the class of membrane-

Electronic supplementary material The online version of this article (doi:10.1007/s10858-012-9684-8) contains supplementary material, which is available to authorized users.

J. Stehle · H. Schwalbe (✉)
Institute for Organic Chemistry and Chemical Biology, Goethe University Frankfurt, 60438 Frankfurt, Germany
e-mail: schwalbe@nmr.uni-frankfurt.de

J. Stehle · F. Löhr · S. Reckel · C. Roos · M. Blum · C. Glaubitz · V. Dötsch · H. Schwalbe
Center of Biomolecular Magnetic Resonance, Goethe University Frankfurt, 60438 Frankfurt, Germany

F. Scholz · M. Braun · J. Wachtveitl
Institute of Physical and Theoretical Chemistry, Goethe University Frankfurt, 60438 Frankfurt, Germany

F. Löhr · S. Reckel · C. Roos · M. Blum · C. Glaubitz · V. Dötsch
Institute of Biophysical Chemistry, Goethe University Frankfurt, 60438 Frankfurt, Germany

embedded light-sensing proteins. They are involved in two of the most fundamental features of membranes in biology, i.e. active transport and sensory signaling. Microbial retinal-binding proteins have been extensively studied (Bogomolni and Spudich 1982; Matsuno-Yagi and Mukohata 1977; Oesterhelt and Stoeckenius 1973; Schobert and Lanyi 1982; Takahashi et al. 1985) and can be subdivided into two general classes, ion pumps and phototaxis receptors. Bacteriorhodopsin (BR) and halorhodopsin (HR) are the most prominent examples for light-driven ion pumps. Phototaxis receptors include sensory rhodopsin I and sensory rhodopsin II (Bogomolni and Spudich 1982; Takahashi et al. 1985). The number of known homologous systems is in the range of ~800. The presence of these systems in all three kingdoms of life, Archaea, Prokarya, and Eukarya, reflects the ubiquitous importance of these light-driven processes.

The retinal-binding protein proteorhodopsin is found in marine proteobacteria. Initial experiments suggested that PR is a light-driven proton pump with pH-dependent vectoriality; at acidic pH PR mediates inward proton pumping whereas at alkaline pH the pumping process can be inverted into an outward pumping of protons (Beja et al. 2001; Friedrich et al. 2002). Its functionally important residues include amino acids D97, the primary proton acceptor, E108, the proton donor, K231 that forms a Schiff base to the chromophore retinal, R94 and D227 that together with D97 act as counterions of the Schiff base (Friedrich et al. 2002). A special feature of PR is the unusually high pKa value of its primary proton acceptor, which is correlated to the pH-dependent formation of a hydrogen bond between D97 and H75 (Friedrich et al. 2002; Hempelmann et al. 2011).

The NMR solution structure of PR in diC7PC, forming a micelle, has recently been solved and revealed a structure of seven transmembrane helices with a hydrophobic core pocket binding the retinal (Reckel et al. 2011). PR has a very similar architecture compared to the previously published structures of retinal-binding proteins (Gautier et al. 2010; Luecke et al. 1999, 2008).

With regard to its dynamic properties, early models of receptors and transporters suggest an on/off state-based mechanism with substantial structural rearrangements within receptors upon activation (Devos et al. 1985; Freire 1998; Leff 1995). However, instead of switching between clearly defined states, a shift in the dynamics of a conformational ensemble might take place emphasizing the essential functional role of conformational dynamics in signal transduction after light excitation. Furthermore, conformational equilibria can be closely coupled to environmental parameters. For BR, large structural rearrangements were observed that were, however, later found not to be a necessary prerequisite for the pumping activity of BR as indicated by mutational studies (Lanyi 2004; Neutze et al. 2002). Similar results were found for sensory rhodopsin II. Only minor structural changes are necessary for SRII to interact with its transducer protein (HtrII) (Sudo and Spudich 2006; Klare et al. 2006). It seems not to be a strict requirement for a protein to undergo conformational changes to induce allostery. Rather, allosteric effects can apparently be induced by modification of the structural dynamics. Therefore, both structural as well as the dynamic changes have to be characterized to gain further insights into allosteric processes important for membrane signaling.

In the present work, we characterize the ground state dynamics of the green-absorbing variant of proteorhodopsin (green PR) solubilized in detergent micelle and utilize our previous optimization of PR solubilization (Fig. 1), NMR chemical shift assignments and structure determination for the analysis. A detergent micelle preparation was used for PR, since it results by far in the best NMR spectra quality. NMR spectroscopy can map different time ranges and amplitudes of conformational dynamics (Reckel et al. 2011).

Heteronuclear overhauser enhancements (hetNOE) are sensitive to dynamics that are substantially faster than the overall rotational correlation time and therefore typically report on dynamics on the sub-nanosecond time scale. Exchange between different conformational states can be monitored by characterizing the field dependence of transverse relaxation rates that affect the intensity of NMR signals. Differences in line widths report on dynamics in the range of micro- to milliseconds, while hydrogen exchange rates are modulated by dynamics occurring on the millisecond to minutes time range. Conformational dynamics in β-sheet membrane proteins have been characterized previously by the groups of Kay, Griesinger and Zweckstetter (Hwang

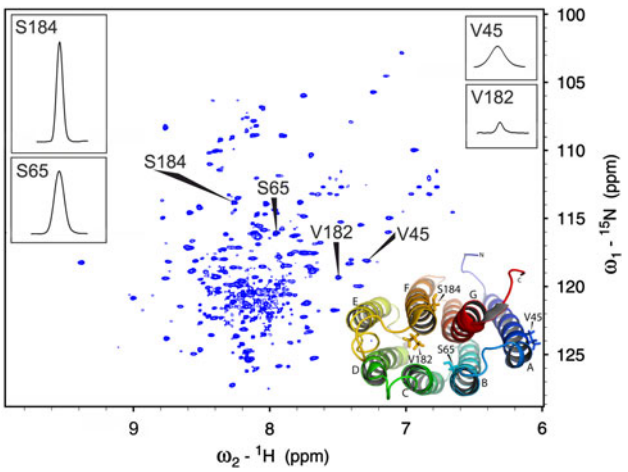

Fig. 1 [^{15}N,^{1}H]-TROSY spectrum of 400 μM PR in diC7PC recorded at pH 5.0, at a ^{1}H Larmor frequency of 700 MHz. 1D *rows* along ω_2 for the resonances of V45, S65, V182, and S184 are shown. NS = 32, 256 complex points in ω_1, 1024 complex points in ω_2, relaxation delay = 1 s, total measurement time: 9 h 7 min

et al. 2004; Villinger et al. 2010). In the present work, we extend such studies to the study of PR, including measurement of ^{15}N heteronuclear NOEs and field-dependent modulation of cross-peak intensities in [^{15}N, ^{1}H]–TROSY experiments. In addition, we compare our data to the dynamics of PR in lipid bilayers as probed by solid-state NMR (Yang et al. 2011). We further characterize pH-dependent ^{1}H and ^{15}N chemical shift changes and report on [^{15}N, ^{1}H]–TROSY experiments with laser-excited PR. The NMR characterization of these dynamics for PR solubilized in detergent micelle are compared with data from optical spectroscopies including transient absorption UV/VIS data, for which we map the impact of different detergents (DDM and diC7PC) on the photocycle.

Based on our data, we can identify distinct regions of the protein that are highly dynamic. We also map out the changes induced by increasing pH from 5 to 9. Our data show that substantial dynamic differences can be detected for PR in detergent micelle at T = 323 K. The dynamics are more pronounced at higher pH, and dynamic hotspots can be identified. Some of the locations of these hotspots coincide with regions of the protein likely to be important for color-tuning and proton pumping.

Materials and methods

Sample preparation

The green absorbing PR was cloned into a pET27+ vector and expressed in the *Escherichia coli* BL21 (DE3) expression system. For PR samples prepared at different pH values, cells were incubated at 37 °C in M9 minimal medium containing ^{15}N enriched ammonium chloride. For the PR samples used in the field-dependent NMR experiments, a ^{2}H, ^{15}N labeled minimal medium (Silantes) was used. Expression (1 liter) was induced with 1 mM IPTG at an OD 600 of 0.7–1. Additionally, 10 μM all-trans retinal was added. After incubation over night at 30 °C (200 rpm), the cell suspension was centrifuged and cells were lysed with a microfludizer: Microfluidics M-110P. After ultracentrifugation for 45 min at 100,000×*g* and 4 °C, the pellet was suspended in 50 mM MES, pH 6, 300 mM NaCl, 5 mM imidazole, 1.5 % (w/v) of dodecyl-β-D-maltoside (DDM) and incubated over night at 4 °C. After ultracentrifugation for 45 min at 100,000×*g* and 4 °C, the supernatant was applied to a HisTrap HP column (GE Healthcare), previously equilibrated with 50 mM MES, pH 6, 300 mM NaCl. The column was washed with ten bed volumes of 50 mM MES, pH 6, 300 mM NaCl, 50 mM imidazole and 0.15 % DDM (w/v). For detergent exchange, the column was washed with 10 bed volumes of 50 mM MES, pH 6, 300 mM NaCl, 50 mM imidazole and 0.15 % (w/v) of 1,2-diheptanoyl-sn-glycero-3-phosphocholine (diC7PC). After eluting with 50 mM MES, pH 7.5, 300 mM NaCl, 50 mM imidazole and 0.15 % (w/v) of diC7PC the sample was centrifuged in a concentrator (cut off 10 kDa) to a volume of 0.5 ml. Buffer was exchanged via a PD 10 column to a phosphate buffer containing 100 mM NaCl for pH values 5, 6.5, and 7; for pH values 8 and 9 a 30 mM Tris buffer containing 100 mM NaCl was used. Concentrating the sample to a volume of 300 μl resulted in a diC7PC concentration of 2 % (w/v) and a protein concentration of 400 μM.

Laser NMR experiments

An argon ion laser with λ = 520 nm (Spectra Physics) was used to illuminate the proteorhodopsin sample. The laser beam was directly guided into the sample within the NMR spectrometer via fiber optical devices (Kuhn and Schwalbe 2000). Continuous wave experiments (Laser was turned on before and during NMR experiments) as well as one shot experiments (Laser illumination with subsequent measurement without continued illumination) were conducted with laser powers ranging from 10 mW to 3 W.

pH dependence of PR

PR samples (protonated) at different pH values were prepared: at pH 5.0, 6.5, 7.5, 8.0, and 9.0 (2 % detergent concentration). For each pH value, a [^{15}N, ^{1}H]–TROSY spectrum was recorded at a 800 MHz Bruker spectrometer for 8 h at T = 323 K. The signal assignment for pH 5 is published (Reckel et al. 2011) and was transferred from pH 5 to all other spectra at different pH values by tracing continuous peak shifts. As a reference 2,2-Dimethyl-2-silapentane-5-sulfonate sodium salt (DSS) was used. For the calculation of the chemical shift perturbations (CSP), Eq. (1) was used.

$$\mathrm{CSP} = \sqrt{(\Delta\omega_H)^2 + (0.1\Delta\omega_N)^2} \quad (1)$$

Magnetic field strength dependence

A 400 μM perdeuterated PR sample at pH 5 was used for the magnetic field strength experiments. [^{15}N, ^{1}H]–TROSY spectra were recorded at 500, 600, 700, 800 and 950 MHz Bruker spectrometers at T = 323 K.

H/D exchange experiments

The H/D exchange at amide sites of proteorhodopsin was followed by recording a series of [^{15}N, ^{1}H]–SOFAST–HMQC (Schanda and Brutscher 2005) spectra after dissolving a freeze-dried sample of the ^{15}N-labeled protonated

protein (50 μM in 2 % diC7PC) in D_2O. Experiments were performed at a temperature of T = 317 K on a 950 MHz spectrometer at pH 5. Recording times of individual spectra were approximately 25 min, the first one being started 10 min after redissolving the protein. To obtain a higher signal-to-noise for unambiguous identification of very slowly exchanging amides a SOFAST–HMQC spectrum was recorded after 26 h with 16 times more scans.

Flash photolysis

The PR-wt samples (1 ml in a fused silica cuvette with optical path length of 1 cm; optical density of 1.0 at 520 nm) solubilized in DDM as well as in diC7PC are optically excited at 520 nm. The pump pulses (pulse width: 20 ns; intensity: 2 mJ/cm^2) are obtained by an optical parametric oscillator (OPO, GWU, laser technic), which is pumped at 355 nm by the third harmonic of a Nd:YAG laser (Spitlight 600 Innolas Laser GmbH). The wavelength of the CW probe beam (white light source: LC8, Hamamatsu) is selected by a monochromator (Photon Technologies International, Inc.). After passing the sample, the transmitted probe beam is guided through a second monochromator to eliminate scattering light resulting from laser excitation. The transmitted intensity is detected using a photomultiplier tube (Photosensor H6780-02, Hamamatsu) and recorded by a digital storage oscilloscope (Waverunner 62xi, LeCroy).

Simulation of the photocycle population dynamics

The obtained flash photolysis data were analyzed following earlier work by Varo et al. (2003). In these simulations, the following sequential photocycle was assumed: $K \rightleftharpoons M_1 \rightarrow M_2 \rightleftharpoons N \rightleftharpoons PR\,(O) \rightarrow PR$, where the spectra of the intermediate states M_1 and M_2 were assumed to be identical as well as of the intermediate states PR (O) and PR. The spectra of the intermediate states and the rates were fitted by a Levenberg–Marquardt algorithm and the respective values by Varo et al. (2003) where chosen as starting point of the fitting process. The system of coupled linear differential equations was solved numerically, yielding calculated transient traces at different experimental probe wavelength, which were then fitted to the flash photolysis data.

Results and discussion

Dynamics of proteorhodopsin in diC7PC at pH 5

Heteronuclear NOE

Modulation of ^{15}N heteronuclear Overhauser effects stem from internal motions that are substantially faster than the overall correlation time; PR in the diC7PC micelle tumbles with an overall correlation of $\tau_c = 24$ ns (at T = 323 K) (Reckel et al. 2011). Helices show no significant enhanced dynamics with the exception of the center part of helix G, adjacent to the covalent attachement of the retinal. The heteronuclear NOE data indicate enhanced flexibility in the C-terminal and N-terminal part of the protein and the loop regions. Flexibility at the C- and N-termini of proteins is common and can be explained by tailing effects at both ends of the protein. The loop regions, however, are not equally affected. Loops AB, BC, CD, and DE experience only small heteronuclear NOE deviations from the theoretical maximal value of ~0.83. The EF loop and especially the FG loop, however, show low heteronuclear NOEs indicating high flexibility (Fig. 2).

Magnetic field strength dependence of NMR signal intensities

In NMR spectroscopy, relaxation and the impact of chemical exchange processes are sensitive to the magnetic field strength. For soluble proteins with high signal-to-noise in ^1H, ^{15}N heteronuclear correlation experiments, measurement of ^{15}N–R_2, ^{15}N–$R_{1\rho}$ and relaxation dispersion are powerful tools to quantify exchange processes. For the large membrane protein PR, solubilized in detergent micelle, we could not perform such in-depth experiments due to insufficient signal-to-noise and very high relaxation rates present already in the coherence transfer steps of the experiments. In addition, peak intensities varied considerably over the sample (Fig. 1). Optimization of detergents used for the liquid-state NMR experiments was previously reported (Reckel et al. 2011) and change from diC7PC to a different detergent, e.g. DDM, yielded significantly worse NMR spectra (see Fig. S1 in Suppl. Mat.). We therefore decided to monitor conformational exchange processes that are intermediate on the chemical shift timescale (micro- to millisecond timescale) by measurement of TROSY experiments at different fields. We quantified cross peak intensities in TROSY spectra at five different ^1H Larmor frequencies: 500, 600, 700, 800, and 950 MHz. Since intensities are affected by a number of different parameters, we normalized the intensities of all residues relative to the intensity of the cross peaks for G21 as a residue with no notable field-dependence in cross peak intensity. Such referencing assumes a constant TROSY effect and equal longitudinal relaxation rates for all residues; this assumption is certainly not strictly valid for all residues but it is the closest possible description available. The relative intensities as a function of residue number at the five field strengths are shown in Fig. 2a. The relative intensities of cross peaks vary by almost one order of magnitude for different residues in PR. Dynamics on the μs–ms time scale is almost exclusively

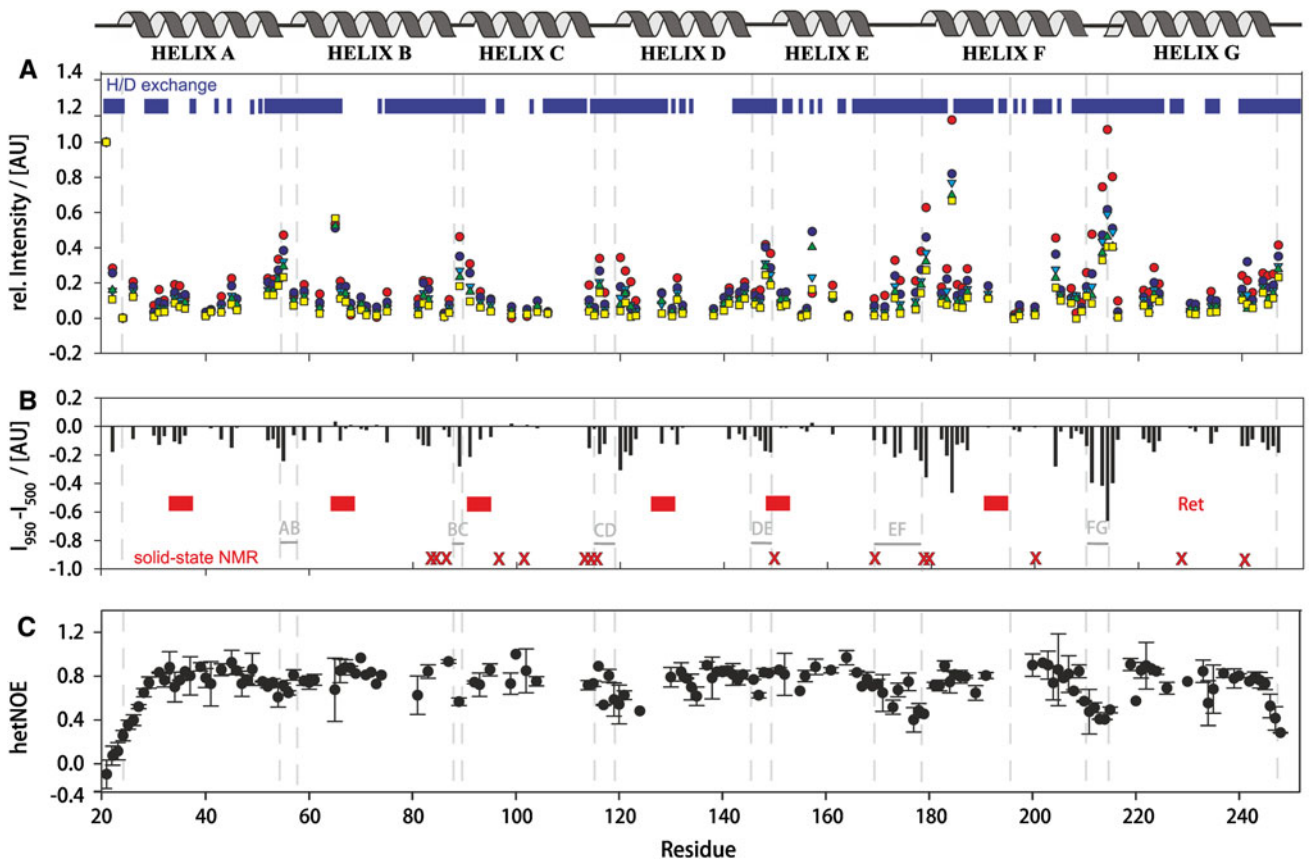

Fig. 2 Magnetic field strength dependence of NMR signal intensities and hetNOEs of 400 μM perdeuterated (**a**, **b**) and protonated (**c**) PR in diC7PC. **a** Relative signal intensities as a function of residue number at ^{1}H Larmor frequencies of 500 MHz (*red*), 600 MHz (*blue*), 700 MHz (*cyan*), 800 MHz (*green*), and 950 MHz (*yellow*). Regions that show H/D exchange are sequentially highlighted by *horizontal blue bar*. **b** Plot of the resonance intensity difference (I950-I500) as a function of residue number. Loop regions (AB, BC, CD, DE, EF, and FG) are indicated as well as the position of retinal covalently attached to K231 (Ret) and residues in contact with retinal (*red boxes*). Differences in ^{13}C-signal intensities due to phase transition from gel-phase to fluid-phase observed by solid-state NMR spectroscopy on PR in DMPC bilayers are depicted as red crosses (Yang et al. 2011). (C) ^{15}N heteronuclear NOE effects indicating flexible regions including the EF and FG loops. For original data see Table S1 in Supplementary Information

limited to regions coinciding with loops in the PR structure. Additionally, portions of helices A and G adjacent to the N- and the C-terminus, respectively, seem to show moderate conformational exchange (Fig. 3).

Interestingly, one of the most prominent effects is visible for residues within helix F (V182-N187). This portion of helix F is adjacent to the very mobile EF-loop as well as the C-terminal portion of helix G, in agreement with the structural ensemble obtained from NMR structure calculations (Reckel et al. 2011). Both the EF and FG loops show significant flexibility, consistent with the obtained ^{15}N heteronuclear NOE data (Fig. 3).

H/D exchange experiments

Experiments that map out amide sites that are labile to exchange with the solvent (H/D exchange experiments) were conducted to investigate the solvent accessibility of amide protons. H/D exchange is sensitive to structural dynamics in the millisecond to second regime. Regions in PR that show solvent exchange are sequentially highlighted in a horizontal blue bar (Fig. 2a) and coincide with all loop regions as well as most parts of helix F and helix G and the C-terminal part of helix A (Fig. 3d). The experiments map out increasing dynamics in almost all parts of the protein on the time regime of up to seconds.

Characterization of pH-dependence of conformational dynamics

The increase of pH leads to a change in the vectoriality of proton pumping in PR (Friedrich et al. 2002; Lorinczi et al. 2009). Friedrich et al. reported that PR acts as a net inward proton pump at acidic pH, and as an outward proton pump at alkaline pH (Lorinczi et al. 2009). Therefore, we investigated pH-dependent changes in the H, N cross peaks

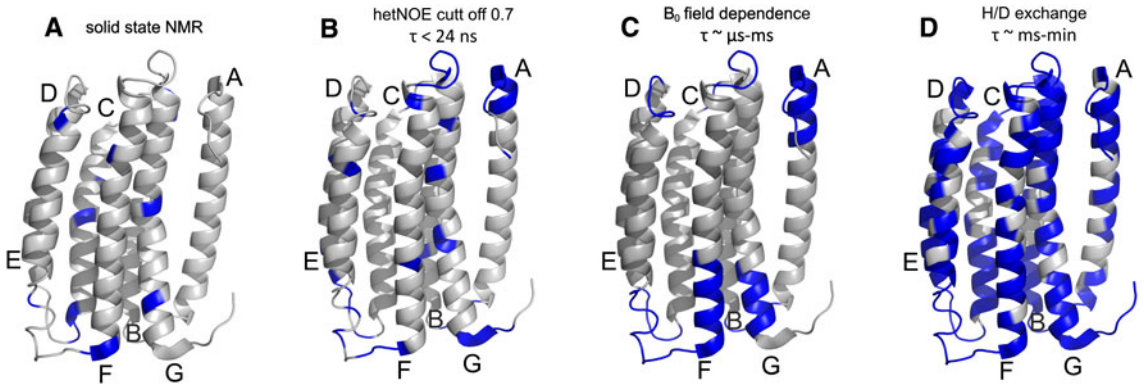

Fig. 3 NMR mapping of dynamics of 400 µM PR in diC7PC over different time regimes. **a** Line broadening as a function of lipid phase transition from gel-phase to fluid-phase observed by solid-state NMR spectroscopy mapped on structure (*blue*) (Yang et al. 2011). **b** ^{15}N heteronuclear NOEs of PR mapped on structure with a cut-off value of 0.7 (*blue*). Heteronuclear NOEs are sensitive to motions substantially faster than the overall rotational correlation time $\tau_c = 24$ ns determined previously (Reckel et al. 2011). **c** Field dependence mapped on structure. Regions showing significant effects at different field strength (see Fig. 2) are colored in *blue*. (D) H/D exchange mapped on structure. Regions in *blue* represent H/D exchange; regions in *grey* represent amino acids that can still be detected after 26 h of H/D exchange. The presentation of the structure was generated using the PyMOL software package (PDB ID: 2X6L). For original data see Table S1 in Supplementary Information

and recorded [^{15}N, ^{1}H]-TROSY spectra at five different pH values, 5.0, 6.5, 7.5, 8.0, and 9.0 at a ^{1}H Larmor frequency of 800 MHz. In general, we found a decrease in the number of backbone amide resonances that can be observed when changing pH from 5.0 to 9.0; the analysis is hampered because signal assignments could only be transferred incompletely due to spectral overlap and only unambiguously transferable signals were considered for the analysis. Not all CSPs showed a linear shifting behavior (see Fig. S2 Suppl. Mat.).

pH-induced CSP were analyzed for each pH step and are shown in Fig. 4a–d. The CSPs for detectable signals range up to 0.10 ppm. For the titration step from pH 8.0 to pH 9.0, the largest detectable shifts are around 0.04 ppm; therefore, we defined this value as lower limit for a significant change. The small size of the observed effect shows that the structure maintains mostly unaffected at the different pHs. Annotating CSPs above 0.04 ppm onto the PR structure (Fig. 5), however, reveals spatial clustering of residues with significant changes.

The size of the detectable CSPs are highly pH-dependent and are generally more prominent at steps from pH 5.0 to pH 6.5 and from pH 6.5 to 7.5, whereas the pH steps from pH 7.5 to pH 8.0 and pH 8.0 to pH 9.0 show only minor CSPs. The most intense CSPs for the first titration step (pH 5.0–pH 6.5) are detected at the EF loop region, the N-terminal part of helix F. Although the effect of enhanced solvent exchange at increasing pH will certainly affect cross peak intensities, we argue that in protein NMR of well folded proteins in regular secondary structure elements even at slightly basic pH, the effect is not prominent. Therefore, we tentatively also analyzed resonances that are lost due to line broadening, presumably due to enhanced dynamics, an accumulation of affected resonances are detected at the N-terminal part of helix F underlining its high pH sensitivity. Another clustering of resonances disappearing with increasing pH in combination with strong CSPs can be observed in the BC loop region as well as in the C-terminal part of helix G, which is highly consistent with the obtained solid-state NMR data (Fig. 2b). Mutational studies in other retinal-binding proteins indicate that the BC loop is involved in the structural stability of the protein and is of crucial importance for retinal binding (Anukanth and Khorana 1994; Doi et al. 1990). Additionally, the N-terminal part of helix D shows an accumulation of disappearing signals. The EF loop which seems to be highly pH sensitive possibly plays a role both in the color tuning mechanism and proton pumping (Yamada et al. 2010). The N-terminal part of helix F is located in close spatial proximity to the EF loop as well as to the C-terminal part of helix G. The sensitivity of this region of the structure in PR to pH-induced changes is in agreement with observations from the magnetic field strength-dependent analysis as well as the heteronuclear NOE data and the solid-state NMR experiments, providing consistent data underlining the significance of this dynamic hotspot for PR function. Furthermore, our data of a mild pH-dependence of the structure of PR are consistent with low-temperature (T = 250 K) FTIR spectroscopy data showing differences in the FTIR absorbance spectra between pH 5.1 and pH 5.5 (Verhoefen et al. 2011). In the pH step from pH 6.5 to pH 7.5, the overall CSPs of the protein slightly increase in number. However, a significant larger number of cross peaks cannot be detected, further supporting the notion that loss of signals in the first titration step is due to increased dynamics. The most affected residues are located in the EF loop region; both, large CSPs and

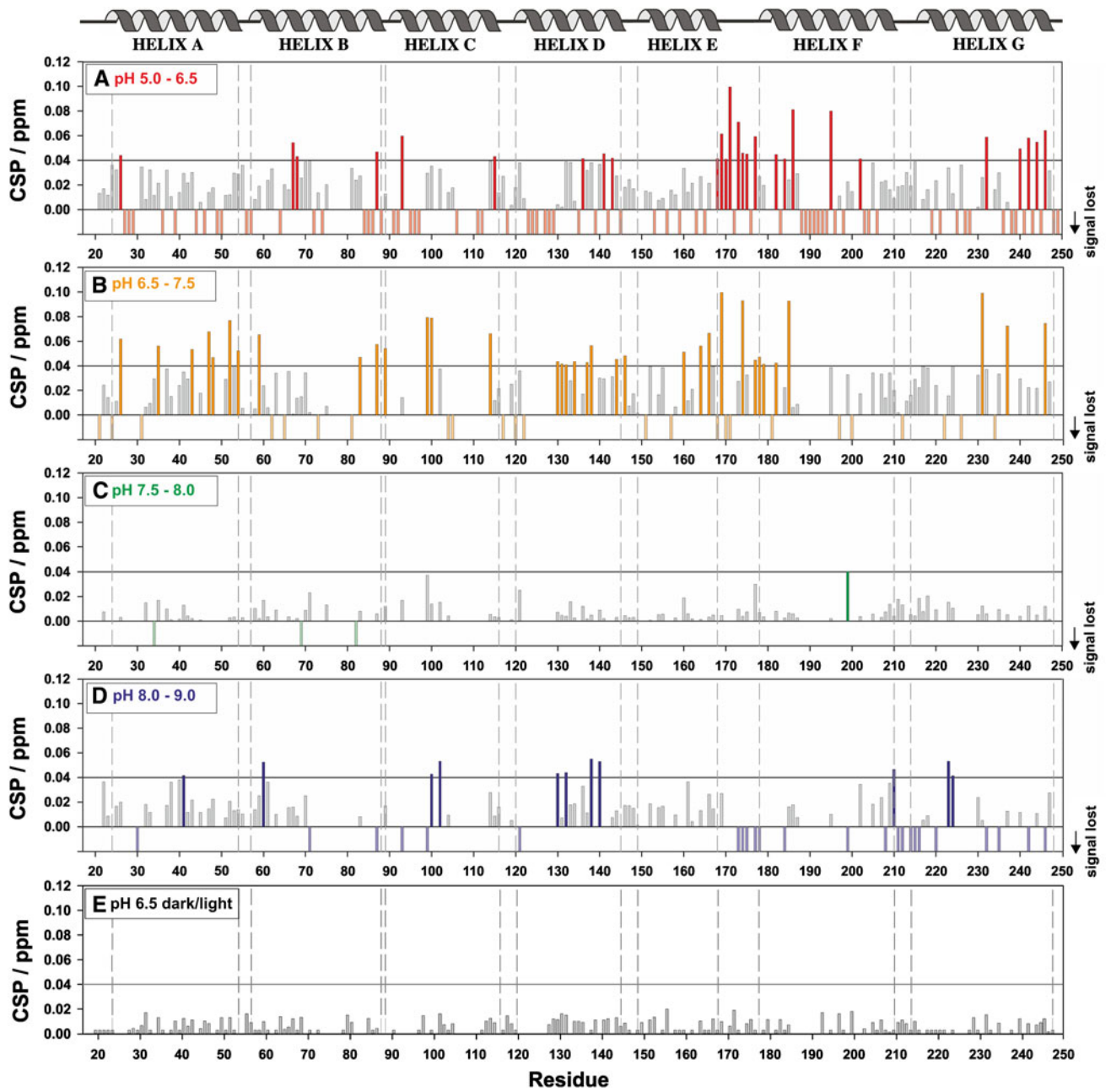

Fig. 4 pH-dependence of 400 μM protonated PR in diC7PC monitored by pH-induced chemical shift perturbations (CSPs). **a** pH 5.0–6.5, **b** pH 6.5–7.5, **c** pH 7.5–8.0, and **d** pH 8.0–9.0. CSPs above a threshold of 0.04 ppm (*horizontal lines*) are colored in *red* (**a**), *orange* (**b**), *green* (**c**), and *blue* (**d**). Resonances that become undetectable due to *line broadening* are shown as *negative bars* colored *pale red* (**a**), *pale orange* (**b**), *pale green* (**c**), and *pale blue* (**d**). Position of helices and loops are depicted and visualized by *vertical dashed lines*. **e** Light induced CSPs of PR resonances at pH 6.5. For original data see Table S1 in Supplementary Information

lost signals are detected. Major CSPs are also detected for residues A185 and K231. For A185, the adjacent residue Y186 shows a large CSP in the pH step from pH 5.0 to pH 6.5, but only a minor CSP in the next pH step, whereas residue A185 shows an opposite behavior. Both residues are located in close spatial proximity opposite the EF loop. For K231, a very large CSP is detected without significant sequential accumulation of other residues that show CSPs. The retinal is covalently bound to the side chain of K231 via a Schiff base. The CSP of >0.1 ppm indicates a significant change for K231 in this pH titration step. At lower pH ranges as well as at higher pH ranges only minor CSPs for K231 are observed. Further accumulation of CSPs can be observed in the AB loop region. Six titratable groups are

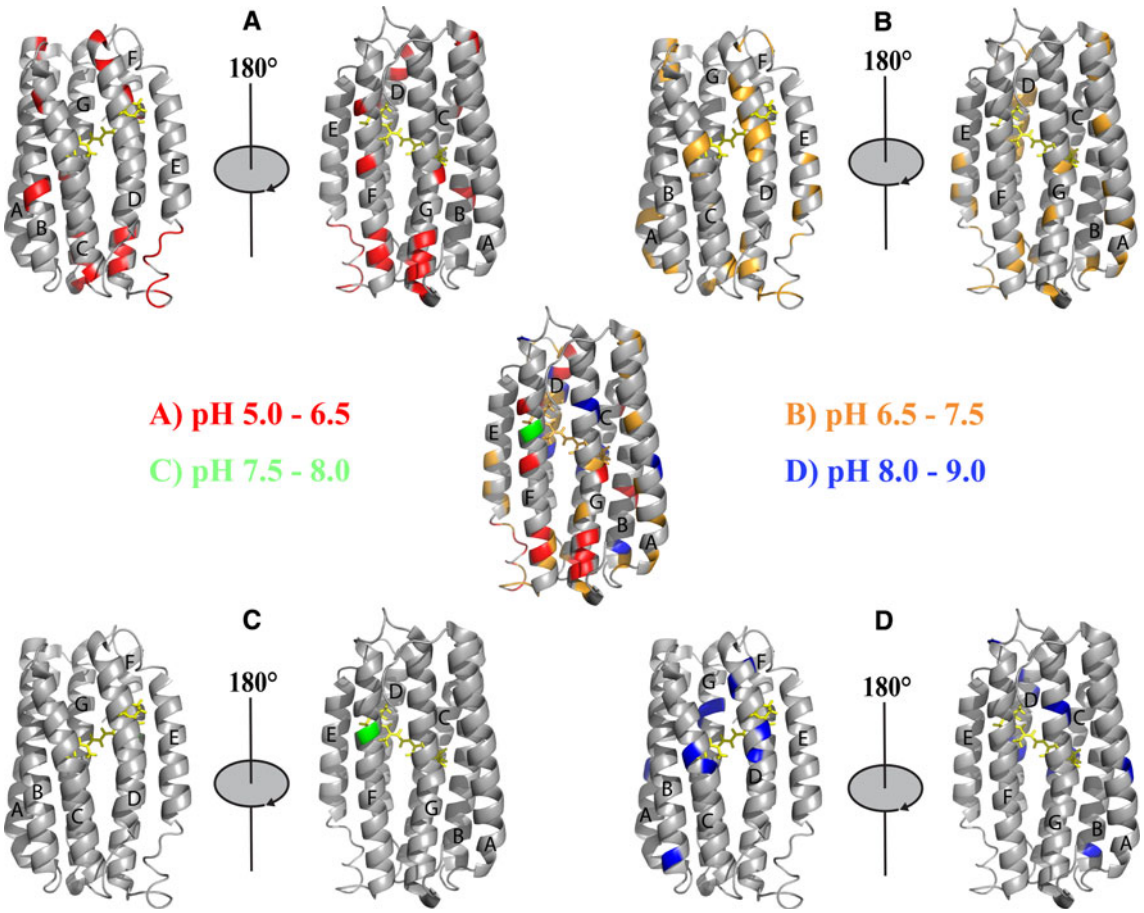

Fig. 5 pH dependence of NMR signals of 400 μM protonated PR in diC7PC mapped onto structure. **a** pH 5.0–6.5, **b** pH 6.5–7.5, **c** pH 7.5–8.0, and **d** pH 8.0–9.0. Regions showing significant effects upon pH shift (see Fig. 4) are colored in *red* (**a**), *orange* (**b**), *green* (**c**), and *blue* (**d**). Structure was generated using the PyMOL software package (PDB ID: 2X6L). For original data see Table S1 in Supplementary Information

located in this region: E50, R51, D52, R53, K57, and K59 indicating a high sensitivity due to pH change. Interestingly, the ERDR part consists of amino acids with alternating acidic (~ 4.1 for E and ~ 3.9 for D) and basic (~ 12.5 for R) pK_a values. For the next pH step from 7.5 → 8.0, only minor CSPs are detected. Notably in the pH step from 8.0 → 9.0, a combination of lost signals as well as two of the few significant CSPs at that pH step can be observed in the FG loop region indicating a stronger influence at higher pH values as compared to lower pH values in this region of the protein. An accumulation of lost signals due to line broadening can also be observed in the EF loop again stressing the pH sensitivity of this region. In other parts of the protein there are no large CSPs, accumulations of CSPs or lost signals in this pH region. The accumulated dynamical changes of PR at higher pH could also possibly be correlated with the protonation state of the highly conserved His75, which forms a stabilizing H-bond with Asp97, the primary proton acceptor explaining its unusually high pKa value (Hempelmann et al. 2011).

Comparison to solid-state NMR experiments

A number of MAS-NMR studies have been carried out to probe structure and dynamics of PR within lipid bilayers (Yang et al. 2011; Shi et al. 2009a, b). Here, we compare our data obtained from detergent micelles with those reported by some of us before on DMPC/DMPA lipid bilayers at 4 °C and at pH 8.5 (Yang et al. 2011). In this study, mobile regions in PR were identified and mapped onto its topology by comparing dipolar cross polarization and scalar INEPT transfer experiments, which differentiate between low mobility regions from those undergoing fast, large amplitude fluctuations. Their coupling to the lipid environment was further visualized by utilizing changes in the bilayer dynamics when undergoing a transition from its gel to the liquid crystalline phase. As shown by Yang et al. (2011), a number of cross peaks disappear from 2-D, cross-polarized CC–DARR spectra. This disappearance is caused by reduced cross polarization efficiency, increased conformational exchange or altered spin diffusion dynamics,

which all respond sensitively to an increase in local dynamics in the fluid bilayer phase. It was found that N- and C-terminal tails, AB loop, BC loop, CD loop and FG loop undergo fast, large amplitude fluctuations. Upon changing bilayer elasticity by switching to the liquid crystalline phase (30 °C), some resonances from the BC loop, from helix C, helix E, EF loop, helix F and helix G broaden and disappear from dipolar spectra indicating increasing flexibility in these protein regions. A number of 15 residues showing this behaviour could be unambiguously identified as indicated in Fig. 2b as red crosses for comparison. The experimental situation in solution NMR experiments described here at higher temperature in detergent micelles is different but similar trends are observed in both situations. Dynamics detected in the solid-state data and the heteronuclear NOE from the liquid state NMR data consistently report that dynamics are observed for functionally relevant parts of PR, such as the EF loop, the N-terminal part of helix F and the C-terminal part of helix G (Yamada et al. 2010). The same consistency can be observed when comparing the magnetic field strength dependence in solution NMR with the dynamics obtained from solid state data (Fig. 2b, c). Minor differences in the obtained dynamic data of solution NMR compared to solid state NMR experiments could be generally due to different experimental conditions, probably mostly due to the use of DMPC/DMPA lipids in solid-state NMR as compared to the use of diC7PC detergent. DMPC/DMPA lipids form lipid bilayers whereas diC7PC keeps PR in solution be forming a micelle. These two systems exert different lateral pressures on PR, a possible explanation for the minor dynamic differences observed.

NMR laser and flash photolysis experiments

The photocycle dynamics of PR are well investigated (Dioumaev et al. 2002; Friedrich et al. 2002; Krebs et al. 2002; Lakatos et al. 2003; Ranaghan et al. 2011; Varo et al. 2003); they exhibit distinct spectral dynamics (see Fig. S3 in Suppl. Mat.). At 590 nm, a decrease of absorption is observed with life times in the μs-time range that can be attributed to the decay of the K-intermediate. This decrease is accompanied with an increase of absorption monitored at 400 nm, typically assigned to a deprotonated Schiff base species (M-intermediate). The decay of M-intermediate is connected with a rise of absorption monitored at 590 nm attributed to the lifetime of the N/O intermediates. At 510 nm, ground state depletion leads to the observation of a negative absorption. The temporal absorption changes at this wavelength are mainly caused by a different spectral overlap of the different intermediates and the dark-adapted state. The signal at all probe wavelengths decays to zero within hundreds of milliseconds, suggesting that the photocycle is completed on this timescale. In the present work, we investigated the dynamic properties of proteorhodopsin also utilizing NMR spectroscopy under sample illumination. For that purpose, we used a set up that allowed direct illumination of the PR sample within the NMR spectrometer via an argon ion laser that was directly connected with the sample through a glass fiber. Different illumination schemes could be applied to the sample and measurements could be conducted in a time-resolved manner. We speculated that continuous illumination might result in successive accumulation of the slowest intermediates present in PR, the N/O intermediates. Values from 10 to 100 mW in 10 mW steps and from 100 mW to 3 W in 100 mW steps have been applied over a time period of 4–8 h respectively and [^{15}N, ^{1}H]–TROSY spectra have been recorded. A more sophisticated version has also been recorded with different illumination times that were directly controlled within the NMR experiment and recorded in a pseudo 3D interleaved manner. The experiments have been conducted at different pH values (between 5.0 and 9.0) because the dynamic behavior of PR is highly sensitive to pH changes (Friedrich et al. 2002). Analyzing the data for the different illumination strengths as well as for the different pH values, only minor changes in the chemical shifts (CSP < 0.02 ppm) could be observed (Fig. 4e), with effects smaller than the CSPs induced by pH. No clear correlation between illumination strength and pH could be identified. Sample heating effects could be excluded by recording ^{1}H-1D control spectra with and without laser irradiation. As a positive control for the activity of PR under the conditions optimized for NMR spectroscopy, we conducted flash photolysis measurements monitoring the PR photocycle (Reckel et al. 2011). In other words, under conditions, where light changes could be observed by flash photolysis experiments, no changes in NMR signals were detected. The photocycle dynamics of PR in DDM are different from diC7PC, a detergent optimal for NMR spectroscopy. At 590 nm, a similar decay of the population of the K-intermediate can be observed, connected to a rise of absorption monitored at 400 nm. In contrast to PR solubilized in DDM, the M-intermediate decays within 100 μs in diC7PC to a constant amplitude of below 20 % which can be observed until the end of the photocycle. Also at 590 nm, a constant amplitude in this time range and no accumulation of N/O-intermediates are observed. For a more quantitative analysis, we fit a kinetic reaction model on the experimental data set, exhibiting the spectral characteristics and the time-dependent population of its photo-intermediates. Consequently, the transient absorption changes obtained by flash photolysis (for more details see Supplementary Information) can be simulated by varying the time-dependent population changes of the photointermediates and the corresponding wavelength-

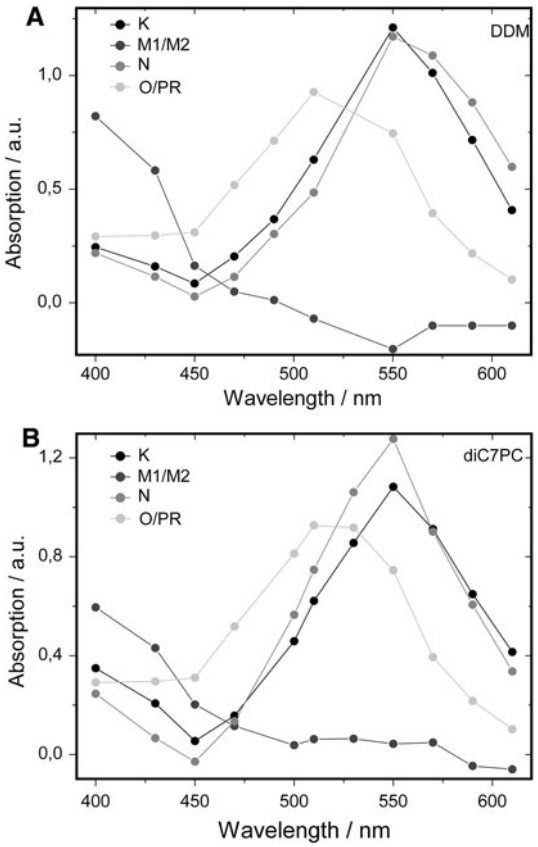

Fig. 6 Simulation of the absorption spectra of PR and its photo intermediates. The flash photolysis data (see supplementary information) are fitted with a kinetic reaction model discussed in Materials and Methods. **a** PR solubilized in DDM. **b** PR solubilized in diC7PC. The spectra of M_1/M_2 and O/PR are identical

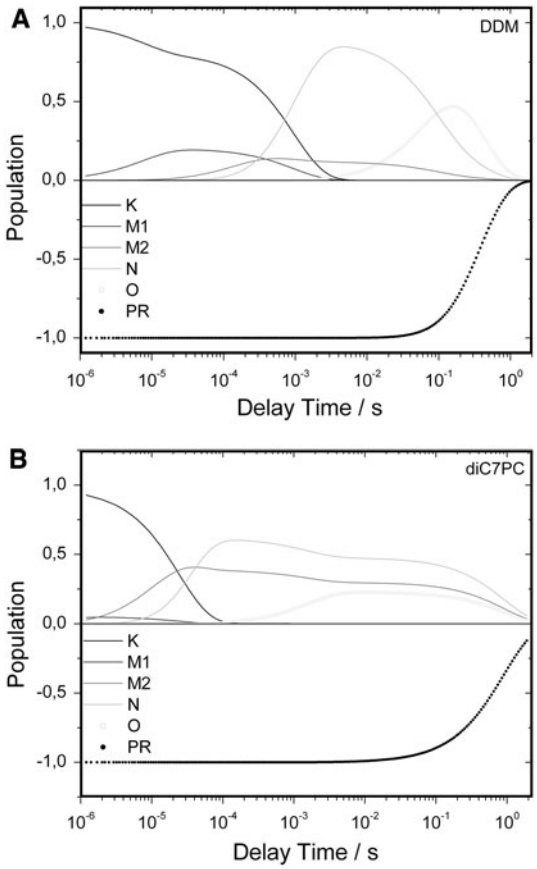

Fig. 7 Simulation of the photocycle population dynamics. Here, the time dependent population changes are shown for **a** PR in DDM **b**: PR in diC7PC. Multiplication of the absorption spectras for PR and its photointermediates (Fig. 6) with the population dynamics (this figure) re-establish the transient absorption changes obtained from flash photolysis

dependent extinction coefficient. The multiplication of the calculated absorption spectra (Fig. 6) with the time dependent population changes (Fig. 7) re-establish the transient absorption changes obtained by flash photolysis. Both data sets (for DDM- or diC7PC-solubilized PR) can be simulated with the same fundamental photocycle involving the same number of intermediates as proposed by Varo et al. (2003). In contrast to the individual interconversion rates of the photocycle intermediates, the absorption spectra of the initial PR state and its photointermediates are not affected by the detergent (Fig. 6).

Therefore, the different dynamics displayed in Fig. 7 are only caused by differences in the populations of the accumulated intermediates. For PR solubilized in DDM, an accumulation of the N-intermediate can be observed. Furthermore, the M_1 state decays on a millisecond-time scale, while only very small amounts of the M_2 state are present until the end of the photocycle. This photocylce is tremendously altered in case of PR solubilized in diC7PC. The temporal population changes of the M_2 and the N state are similar. On a millisecond-time scale, the O state is populated, displaying a dynamic decay similar to the M_2 and the N state. The data suggest an equilibrium with similar populations for M_2, N and O photo-intermediates. Our analysis shows that in diC7PC, the M_2, N/O, and O intermediates exist in an equilibrium during most of the time of the photocycle, which probably explains the lack of significant effects in the NMR spectra under illumination. It would be interesting to determine the origin of the markedly altered photodynamics we detected in the photocycle of PR in DDM and diC7PC. Due to high similarity of the spectral characteristics, we rule out massive difference in the conformations that influence the photocycle. One explanation might be a possible charge effect. diC7PC is zwitterionic, whereas DDM is neutral. Due to the fact that while M_2, N, and O intermediates are populated, mainly the Schiff base (M) and the primary proton acceptor (N) is reprotonated from the aqueous bulk phase, a charged detergent might interfere with these protonation steps, notably by prolonging the lifetime of these states. Other aspects that possibly influence the photocycle characteristics are the chain length of the detergent, its glycerol

backbone, and the number of its acyl chains. Different detergents form micelles of different size which is certainly another major factor that explains the discrepancy between DDM and diC7PC. From a mechanistic point of view, certainly the different lateral pressures that are exerted from different detergents on PR also play an important role (Andersson et al. 2009), in particular in lipid bilayers.

PR does not show significant CSPs in the [^{15}N, ^{1}H]–TROSY spectra upon illumination. Under similar conditions, changes in the hydrogen bonding network, either local or more global, can be detected in FTIR experiments at T = 250 K. Reconciliation of these two experimental findings might imply that at T = 323 K, the average conformation of the M, N, and O intermediates does not significantly deviate from the ground state structure of PR. Further, PR might experience no major rearrangements but rather small, subtle changes in its structural dynamics that result in sufficient adjustment to undergo the photocycle.

Conclusions

Here, we present NMR experiments that provide insight into structural and dynamic properties of PR solubilized in diC7PC monitored for time scales between nanoseconds and up to minutes utilizing a variety of different NMR techniques and characterize the pH- and light dependence of these dynamics.

Additionally, we conducted flash photolysis experiments of PR in DDM as well as in diC7PC demonstrating the activity and completion of the photocycle in both systems. Furthermore the obtained data was compared to solid-state NMR experiments previously reported by some of us (Yang et al. 2011). Combining various techniques and numerous experiments a remarkably consistent picture of the structural and dynamic properties of PR arises. The detailed data analysis of solution NMR experiments as well as the comparison to solid-state NMR experiments consistently stresses the correlation of dynamics, mainly in loop regions of the protein, with regions previously reported as important for PR function (Yamada et al. 2010), such as the EF loop, the N-terminal part of helix F and the C-terminal part of helix G. The EF loop is of special interest in this regard. In BR, the EF loop has been shown to undergo an opening motion during the photocycle (Lanyi and Luecke 2001). Such a motion could be also enabled in PR by intrinsic equilibrium fluctuations as shown here in micelles or in lipid bilayers (Yang et al. 2011). It has also been speculated by Shi et al. (2009b) that the high flexibility in the FG loop supports proton release, since in PR, unlike in BR, there is no proton release complex. PR consists of a number of hydrophobic amino acids at its cytoplasmic site, so it seems possible that in PR, similar to BR, water molecules are incorporated into the structure opening up a protonation pathway. During the M_2–N transition in BR mainly helix F is shifted possibly explaining a highly flexible EF-loop in PR. Zooming out from the EF loop region and comparing the heteronuclear NOE data with the field-dependent NMR intensities shows that the dynamics at subnanosecond time scale pertain on the micro- to millisecond time scale (Henzler-Wildman et al. 2007). By contrast, the H/D exchange experiments are widespread throughout the protein and show that for these longer time scales, almost all parts of the proteins are involved in conformational dynamics.

Noteworthy, in line with the differences between various detergents, we cannot observe significant CSPs upon in situ illumination, even though PR is active under the used NMR sample conditions. Our results suggest that the dynamic ensemble of PR experiences only minor, further conformational changes if at all, suggesting a dynamically controlled activation process. These findings are in-line with observations made on allostery induced by dynamic structural changes rather than major conformational changes (Cooper and Dryden 1984; Popovych et al. 2006; Wand 2001). In fact, it was shown that tertiary very subtle structural changes, beyond possible detection in NMR spectroscopy, can be the difference between an active and an inactive state (Koshland 1998). Our data demonstrate that PR in diC7PC only shows subtle CSP effects but slightly more pronounced variations on its conformational dynamics upon pH changes, while no effect upon illumination was observed. The latter can be explained by the specifics of the photocycle kinetics and intermediate state equilibria. But our observations also indicate that changes in conformational dynamics might be functionally as important as sequential changes along structural defined intermediates.

Acknowledgments This work was supported by the DFG-funded Collaborative Research Center 807; DFG-funded Center of Excellence: Macromolecular Complexes; Joint Research Activities in EU-funded project Bio-NMR. We thank Robert Silvers and Tanja Stehle for very insightful discussions.

References

Andersson M, Malmerberg E, Westenhoff S, Katona G, Cammarata M, Wohri AB, Johansson LC, Ewald F, Eklund M, Wulff M, Davidsson J, Neutze R (2009) Structural dynamics of light-driven proton pumps. Structure 17(9):1265–1275. doi:10.1016/j.str.2009.07.007

Anukanth A, Khorana HG (1994) Structure and function in rhodopsin. Requirements of a specific structure for the intradiscal domain. J Biol Chem 269(31):19738–19744

Beja O, Spudich EN, Spudich JL, Leclerc M, DeLong EF (2001) Proteorhodopsin phototrophy in the ocean. Nature 411(6839):786–789. doi:10.1038/35081051

Bogomolni RA, Spudich JL (1982) Identification of a third rhodopsin-like pigment in phototactic Halobacterium halobium. Proc Natl Acad Sci U S A 79(20):6250–6254

Cooper A, Dryden DT (1984) Allostery without conformational change. A plausible model. Eur Biophys J 11(2):103–109

Devos C, Robberecht P, Nokin P, Waelbroeck M, Clinet M, Camus JC, Beaufort P, Schoenfeld P, Christophe J (1985) Uncoupling between beta-adrenoceptors and adenylate-cyclase in dog ischemic myocardium. N-S Arch Pharmacol 331(1):71–75

Dioumaev AK, Brown LS, Shih J, Spudich EN, Spudich JL, Lanyi JK (2002) Proton transfers in the photochemical reaction cycle of proteorhodopsin. Biochemistry 41(17):5348–5358

Doi T, Molday RS, Khorana HG (1990) Role of the intradiscal domain in rhodopsin assembly and function. Proc Natl Acad Sci USA 87(13):4991–4995

Freire E (1998) Statistical thermodynamic linkage between conformational and binding equilibria. Adv Protein Chem 51:255–279

Friedrich T, Geibel S, Kalmbach R, Chizhov I, Ataka K, Heberle J, Engelhard M, Bamberg E (2002) Proteorhodopsin is a light-driven proton pump with variable vectoriality. J Mol Biol 321(5): 821–838

Gautier A, Mott HR, Bostock MJ, Kirkpatrick JP, Nietlispach D (2010) Structure determination of the seven-helix transmembrane receptor sensory rhodopsin II by solution NMR spectroscopy. Nat Struct Mol Biol 17(6):768–774. doi:10.1038/nsmb.1807

Hempelmann F, Holper S, Verhoefen MK, Woerner AC, Kohler T, Fiedler SA, Pfleger N, Wachtveitl J, Glaubitz C (2011) His75-Asp97 cluster in green proteorhodopsin. J Am Chem Soc 133(12):4645–4654. doi:10.1021/ja111116a

Henzler-Wildman KA, Lei M, Thai V, Kerns SJ, Karplus M, Kern D (2007) A hierarchy of timescales in protein dynamics is linked to enzyme catalysis. Nature 450(7171):913–916. doi:10.1038/nature06407

Hwang PM, Bishop RE, Kay LE (2004) The integral membrane enzyme PagP alternates between two dynamically distinct states. Proc Natl Acad Sci U S A 101(26):9618–9623. doi:10.1073/pnas.0402324101

Klare JP, Bordignon E, Doebber M, Fitter J, Kriegsmann J, Chizhov I, Steinhoff HJ, Engelhard M (2006) Effects of solubilization on the structure and function of the sensory rhodopsin II/transducer complex. J Mol Biol 356(5):1207–1221. doi:10.1016/j.jmb.2005.12.015

Koshland DE Jr (1998) Conformational changes: how small is big enough? Nat Med 4(10):1112–1114. doi:10.1038/2605

Krebs RA, Alexiev U, Partha R, DeVita AM, Braiman MS (2002) Detection of fast light-activated H+release and M intermediate formation from proteorhodopsin. BMC Physiol 2:5

Kuhn T, Schwalbe H (2000) Monitoring the kinetics of ion-dependent protein folding by time-resolved NMR spectroscopy at atomic resolution. J Am Chem Soc 122(26):6169–6174. doi:10.1021/Ja994212b

Lakatos M, Lanyi JK, Szakacs J, Varo G (2003) The photochemical reaction cycle of proteorhodopsin at low pH. Biophys J 84(5):3252–3256. doi:10.1016/S0006-3495(03)70049-6

Lanyi JK (2004) Bacteriorhodopsin. Annu Rev Physiol 66:665–688. doi:10.1146/annurev.physiol.66.032102.150049

Lanyi JK, Luecke H (2001) Bacteriorhodopsin. Curr Opin Struct Biol 11(4):415–419

Leff P (1995) The 2-state model of receptor activation. Trends Pharmacol Sci 16(3):89–97

Lorinczi E, Verhoefen MK, Wachtveitl J, Woerner AC, Glaubitz C, Engelhard M, Bamberg E, Friedrich T (2009) Voltage- and pH-dependent changes in vectoriality of photocurrents mediated by wild-type and mutant proteorhodopsins upon expression in Xenopus oocytes. J Mol Biol 393(2):320–341. doi:10.1016/j.jmb.2009.07.055

Luecke H, Schobert B, Richter HT, Cartailler JP, Lanyi JK (1999) Structure of bacteriorhodopsin at 1.55 A resolution. J Mol Biol 291(4):899–911. doi:10.1006/jmbi.1999.3027

Luecke H, Schobert B, Stagno J, Imasheva ES, Wang JM, Balashov SP, Lanyi JK (2008) Crystallographic structure of xanthorhodopsin, the light-driven proton pump with a dual chromophore. Proc Natl Acad Sci U S A 105(43):16561–16565. doi:10.1073/pnas.0807162105

Matsuno-Yagi A, Mukohata Y (1977) Two possible roles of bacteriorhodopsin; a comparative study of strains of Halobacterium halobium differing in pigmentation. Biochem Biophys Res Commun 78(1):237–243

Neutze R, Pebay-Peyroula E, Edman K, Royant A, Navarro J, Landau EM (2002) Bacteriorhodopsin: a high-resolution structural view of vectorial proton transport. Biochim Biophys Acta 1565(2):144–167

Oesterhelt D, Stoeckenius W (1973) Functions of a new photoreceptor membrane. Proc Natl Acad Sci U S A 70(10):2853–2857

Popovych N, Sun S, Ebright RH, Kalodimos CG (2006) Dynamically driven protein allostery. Nat Struct Mol Biol 13(9):831–838. doi:10.1038/nsmb1132

Ranaghan MJ, Schwall CT, Alder NN, Birge RR (2011) Green proteorhodopsin reconstituted into nanoscale phospholipid bilayers (nanodiscs) as photoactive monomers. J Am Chem Soc 133(45):18318–18327. doi:10.1021/ja2070957

Reckel S, Gottstein D, Stehle J, Löhr F, Verhoefen MK, Takeda M, Silvers R, Kainosho M, Glaubitz C, Wachtveitl J, Bernhard F, Schwalbe H, Güntert P, Dötsch V (2011) Solution NMR structure of proteorhodopsin. Angew Chem Int Ed Engl 50(50): 11942–11946. doi:10.1002/anie.201105648

Schanda P, Brutscher B (2005) Very fast two-dimensional NMR spectroscopy for real-time investigation of dynamic events in proteins on the time scale of seconds. J Am Chem Soc 127(22): 8014–8015. doi:10.1021/Ja051306e

Schobert B, Lanyi JK (1982) Halorhodopsin is a light-driven chloride pump. J Biol Chem 257(17):10306–10313

Shi L, Ahmed MA, Zhang W, Whited G, Brown LS, Ladizhansky V (2009a) Three-dimensional solid-state NMR study of a seven-helical integral membrane proton pump–structural insights. J Mol Biol 386(4):1078–1093

Shi L, Lake EM, Ahmed MA, Brown LS, Ladizhansky V (2009b) Solid-state NMR study of proteorhodopsin in the lipid environment: secondary structure and dynamics. Biochim Biophys Acta 1788(12):2563–2574. doi:10.1016/j.bbamem.2009.09.011

Sudo Y, Spudich JL (2006) Three strategically placed hydrogen-bonding residues convert a proton pump into a sensory receptor. Proc Natl Acad Sci U S A 103(44):16129–16134. doi:10.1073/pnas.0607467103

Takahashi T, Tomioka H, Kamo N, Kobatake Y (1985) A photosystem other than Ps370 also mediates the negative phototaxis of Halobacterium-Halobium. FEMS Microbiol Lett 28(2):161–164

Varo G, Brown LS, Lakatos M, Lanyi JK (2003) Characterization of the photochemical reaction cycle of proteorhodopsin. Biophys J 84(2 Pt 1):1202–1207. doi:10.1016/S0006-3495(03)74934-0

Verhoefen MK, Schafer G, Shastri S, Weber I, Glaubitz C, Mäntele W, Wachtveitl J (2011) Low temperature FTIR spectroscopy provides new insights in the pH-dependent proton pathway of proteorhodopsin. Biochim Biophys Acta 12:1583–1590. doi:10.1016/j.bbabio.2011.09.001

Villinger S, Briones R, Giller K, Zachariae U, Lange A, de Groot BL, Griesinger C, Becker S, Zweckstetter M (2010) Functional dynamics in the voltage-dependent anion channel. Proc Natl Acad Sci U S A 107(52):22546–22551. doi:10.1073/pnas.1012310108

Wand AJ (2001) Dynamic activation of protein function: a view emerging from NMR spectroscopy. Nat Struct Biol 8(11): 926–931. doi:10.1038/nsb1101-926

Yamada K, Kawanabe A, Kandori H (2010) Importance of alanine at position 178 in proteorhodopsin for absorption of prevalent ambient light in the marine environment. Biochemistry 49(11):2416–2423. doi:10.1021/bi9020204

Yang J, Aslimovska L, Glaubitz C (2011) Molecular dynamics of proteorhodopsin in lipid bilayers by solid-state NMR. J Am Chem Soc 133(13):4874–4881. doi:10.1021/ja109766n